Exploring the spatial resolution of TMS-EEG coupling on the sensorimotor region

Brice Passera, Alan Chauvin, Estelle Raffin, Thierry Bougerol, Olivier David, Sylvain Harquel

NeuroImage 259 (2022) 119419

Contents lists available at ScienceDirect

NeuroImage

journal homepage: www.elsevier.com/locate/neuroimage

Exploring the spatial resolution of TMS-EEG coupling on the sensorimotor region

Brice Passera[a,b,g], Alan Chauvin[b], Estelle Raffin[a,c,d], Thierry Bougerol[a,e], Olivier David[a,f,#], Sylvain Harquel[b,c,d,#,*]

[a] Univ. Grenoble Alpes, Inserm, U1216, Grenoble Institut Neurosciences, Grenoble 38000, France
[b] Univ. Grenoble Alpes, CNRS, UMR5105, Laboratoire Psychologie et NeuroCognition, LPNC, Grenoble F-38000, France
[c] Defitech Chair of Clinical Neuroengineering, Center for Neuroprosthetics (CNP) and Brain Mind Institute (BMI), Ecole Polytechnique Federale de Lausanne (EPFL), Chemin des Mines 9, Geneva 1202, Switzerland
[d] Defitech Chair of Clinical Neuroengineering, Center for Neuroprosthetics (CNP) and Brain Mind Institute (BMI), Ecole Polytechnique Federale de Lausanne (EPFL Valais), Clinique Romande de Réadaptation, Sion, Switzerland
[e] Centre Hospitalier Univ. Grenoble Alpes, Service de Psychiatrie, Grenoble F-38000, France
[f] Aix Marseille Univ, Inserm, U1106, INS, Institut de Neurosciences des Systèmes, Marseille, France
[g] Berenson-Allen Center for Noninvasive Brain Stimulation, Division of Cognitive Neurology, Department of Neurology, Beth Israel Deaconess Medical Center, Harvard Medical School, Boston, MA, United States

ARTICLE INFO

Keywords:
TMS-EEG coupling
Spatial resolution
Sensorimotor cortex
Robotized cortical mapping

ABSTRACT

The use of TMS-EEG coupling as a neuroimaging tool for the functional exploration of the human brain recently gained strong interest. If this tool directly inherits the fine temporal resolution from EEG, its spatial counterpart remains unknown. In this study, we explored the spatial resolution of TMS-EEG coupling by evaluating the minimal distance between two stimulated cortical sites that would significantly evoke different response dynamics. TMS evoked responses were mapped on the sensorimotor region in twenty participants. The stimulation grid was composed of nine targets separated between 10 and 15 mm on average. The dynamical signatures of TMS evoked activity were extracted and compared between sites using both local and remote linear regression scores and spatial generalized mixed models. We found a significant effect of the distance between stimulated sites on their dynamical signatures, neighboring sites showing differentiable response dynamics. Besides, common dynamical signatures were also found between sites up to 25-30 mm from each other. This overlap in dynamical properties decreased with distance and was stronger between sites within the same Brodmann area. Our results suggest that the spatial resolution of TMS-EEG coupling might be at least as high as 10 mm. Furthermore, our results reveal an anisotropic spatial resolution that was higher across than within the same Brodmann areas, in accordance with the TMS induced E-field modeling. Common cytoarchitectonic leading to shared dynamical properties within the same Brodmann area could also explain this anisotropy. Overall, these findings suggest that TMS-EEG benefits from the spatial resolution of TMS, which makes it an accurate technique for meso-scale brain mapping.

1. Introduction

Transcranial magnetic stimulation (TMS) is being developed as an exploratory tool for the evaluation of cortical excitability and connectivity (Valero-Cabré et al., 2017), which may be important for the diagnosis of several neurological and psychiatric disorders (Arnaldi et al., n.d.; Bagattini et al., 2019; Bauer et al., 2017; Berlim et al., 2017; Morris et al., 2020; Rehn et al., 2018). Using electromyographic (EMG) recordings, the effects of TMS on the primary motor cortex (M1) have been well described, from the spatial resolution of motor mapping to the effects of repeated TMS (rTMS) on cortical plasticity (Pascual-Leone et al., 2011). The brain responses to single pulse TMS can also be measured with electroencephalography (EEG) (Farzan et al., 2016; Tremblay et al., 2019). Many areas other than M1 have thus been studied, such as the dorsal lateral prefrontal cortex (see e.g. Woźniak-Kwaśniewska et al., 2014), the supplementary motor area (Casarotto et al., 2018), as well as parietal and occipital areas (see e.g. Harquel et al., 2016a; Rosanova et al., 2009). For these targets, the effects of stimulation intensity (Komssi et al., 2004; Raffin et al., 2020), coil orientation (Casarotto et al., 2010), and for M1 the effect of pharmacological agent on neurotransmitters (Premoli et al., 2017, 2014; Ziemann et al., 2015) on TMS evoked brain response have been well characterized. However, an important parameter remains yet to be explored: the spatial resolution of the TMS-EEG approach, i.e., the minimal distance between two stimulated cortical sites resulting in differentiable evoked responses

E-mail address: sylvain.harquel@epfl.ch (S. Harquel).
Co-last authors
* Corresponding author.

https://doi.org/10.1016/j.neuroimage.2022.119419.
Received 27 September 2021; Received in revised form 12 April 2022; Accepted 27 June 2022
Available online 28 June 2022.

dynamics. This characterization is critical for assessing the experimental limits of future fundamental and clinical applications of TMS-EEG mapping.

The spatial resolution of TMS-EMG is well known, mainly because EMG is a straightforward and reliable measure of the TMS induced effect on the cortico-spinal activity (Wassermann et al., 2008). Due to M1 somatotopic organization, experimenters can target a specific muscle on the cortex (Rossi et al., 1998), by finding the target eliciting the largest and most reliable motor evoked response (MEP). This motor hotspot is found by probing the area of M1 corresponding to the muscle based on anatomical landmark, and refining its location by measuring the MEP to its surrounding (Meincke et al., 2016; Rossini et al., 1994; van de Ruit et al., 2015). Several studies showed that the spatial resolution of this technique could be as high as 5-7 mm, a shift of such magnitude causes the TMS pulse to elicit a distinct muscular response (Harquel et al., 2017). Such a resolution allows researchers to precisely map the motor response to TMS in adjacent hand muscles (Säisänen et al., 2021). In doing so, following the central sulcus shape can improve the spatial resolution of motor mapping (Dubbioso et al., 2020; Raffin et al., 2015).

With TMS-EEG, the brain response to TMS can be inferred on most of the superficial cortex. Numerous studies showed that the TMS evoked potential (TEP) is a complex but reproducible signal (Casarotto et al., 2010; Lioumis et al., 2009), although it requires a greater number of trials than MEP to reach an adequate signal-to-noise ratio and is influenced by peripheral confounds (Siebner et al., 2019). In a broad mapping study, we stimulated 18 cortical targets and showed the dynamic signatures specific to different cortical areas (Harquel et al., 2016a). Along with other works (see e.g. Casarotto et al., 2018; Caulfield et al., 2020; Rosanova et al., 2009), this result demonstrated that TMS-EEG can record different response patterns across relatively distant sites, but there is no study to date that properly assesses the spatial resolution of this technique.

While MEP peak-to-peak amplitude is widely used for mapping M1 and defining motor cortical excitability, the equivalent EEG response markers used across studies are differing. They can be the amplitude or latency of TEPs' specific peaks (such as the P30 or N1-P2 complex (Komssi et al., 2004; Roos et al., 2021)) or the time-frequency signature of the induced response (Fecchio et al., 2017). However, all these TEP markers, generally studied at the group level, suffer from large inter-individual and inter-site variability. In a recent study, our team proposed a new way to assess the difference in dynamical properties across sites or conditions, using a linear regression-based marker (RQS) at the single trial level (Raffin et al., 2020). By considering the full dynamic of the signal from 15 ms to 80 ms, this score estimates how much a single TMS-EEG trial contains meaningful EEG signal contributing to the average TEP waveform. In the context of the present study, this analysis captures the specificity of the evoked neural activity across stimulation sites, by exploring the spatial dependency of the quality of this regression across our stimulation grid. This readout is also much less sensitive to inter-individual differences regarding TEPs than when focusing on specific peaks only (Bridwell et al., 2018; Raffin et al., 2020).

Here, to measure the spatial resolution of TMS-EEG, we compared the EEG responses' dynamics over sensorimotor areas from three neighboring Brodmann areas (BA), using a local 3x3 stimulation grid centered over the motor hot-spot. Differences in the global brain response were first assessed by means of global mean field potential (GMFP) as well as topographic analyses. The local evoked dynamics were retrieved from TEPs and analyzed using paired and unpaired RQS. A second aim was to identify factors that would modulate the TMS-EEG spatial resolution. First, the dynamical signature of targets located within the same Brodmann area should overlap between sites thus lowering spatial resolution, due to common cytoarchitectonics (Harquel et al., 2016a). Second, the position of the target within the mediolateral axis might also influence the spatial resolution, due to peripheral evoked potentials (PEPs, (Conde et al., 2018; Roos et al., 2021)). Such peripheral confounds includes auditory evoked potentials (Braack et al., 2015), which could increase as the coil is moved closer to the ears, and sensory evoked potential, which should depend on the laterality of the target, due in part to the differences in scalp muscles implantation (Mutanen et al., 2013). The TEP should also be influenced by the MEPs generating different reafferent sensory input levels depending on the grid site (Biabani et al., 2019; Fecchio et al., 2017). Finally, we correlated these electrophysiological readouts with realistic induced electrical field modelling (Saturnino et al., 2019). In addition to providing another experimental validation of such modelling, it allows to discuss TMS-EEG spatial resolution using the state-of-the-art method to estimate TMS resolution.

2. Material and methods

2.1. Participants

Twenty healthy volunteers (9 males, 25.4±1.4, right-handed) participated in the study. All of them fitted the criteria for MRI and TMS experimentation (Rossini et al., 2015) and gave their informed written consent to participate in the study. Neither of them had a history of psychiatric, neurologic disorders nor alcohol or substance abuse. All of them were free of pharmaceutical impacting cortical excitability. This study was approved by the ethical committee of Grenoble University Hospital (ID RCB: 2013-A01734-41) and registered on ClinicalTrials.gov (number NCT02168413).

2.2. Data and code availability

The data recorded for this study are not publicly available due to absence of public data sharing statement in the informed consent form signed by the participant. The data may be available on request from the corresponding author [SH], on the condition that a data sharing agreement between the academic buyer and Grenoble University Hospital is established. The EEG data analysis function used in this work (using Matlab and Fieldtrip toolbox) can be found here: https://gricad-gitlab.univ-grenoble-alpes.fr/harquels/public_codes.

2.3. Protocol design

MRI and TMS-EEG acquisition took place at the IRMaGe facility of University Grenoble Alpes. Prior to the experiment, each participant underwent a T1 MRI required for the neuronavigation software (Achieva 3.0T TX, Philips, Netherlands; T1TF2, TR = 25 ms, TE = 4 ms, voxel size = 0.95 mm^3 anisotropic). Following the EEG cap set-up, we performed a standard hotspot hunting procedure on the primary motor cortex (M1) for the first dorsal interosseous (FDI). We positioned targets on the posterior and anterior neighboring BA of M1 on BA 4 (i.e. primary sensory cortex S1 on BA 1-2&3, and premotor cortex PM on BA 6 respectively), aligned with the motor hotspot. Lateral and medial targets were placed at least one centimeter from the other targets, leading to a square grid of 9 targets (Figure 1). Targets were defined from medial to lateral with suffix "a" to "c" respectively. The mean distances between S1 and M1 sites, and M1 and PM sites were 12.8 ± 2.2 mm and 15.2 ± 3 mm respectively. On the lateral axis, the mean distances between lines a and b, and b and c were 10.4 ± 1.4 and 10.7 ± 1.5. The TMS experiment was performed by stimulating each of the 9 points of the grid together with a realistic sham condition, while recording concurrently both EEG and MEPs. The sequence of stimulation between targets was randomized between participants.

2.4. TMS parameters

Biphasic TMS pulses were delivered on an anterior to posterior direction by a Magpro Cool AP B65-RO double side (active, placebo) butterfly coil (MagVenture A/S, Denmark) placed tangentially to the scalp

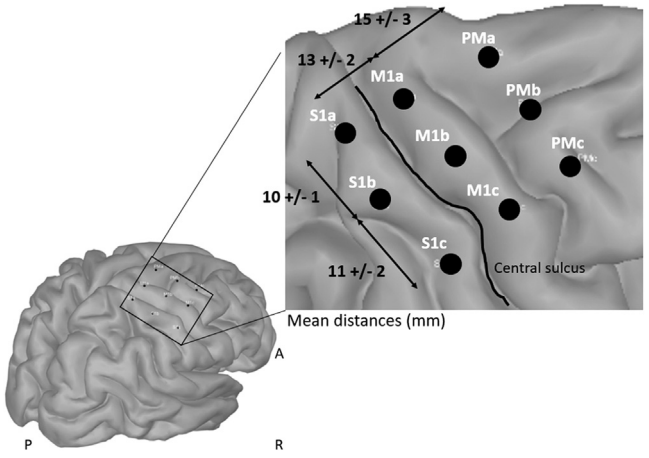

Fig. 1. - Stimulation grid used in the experiment. Sites are sorted by Brodmann areas from the most posterior (S1, BA 1-2&3) to the most anterior (PM, BA 6). On each BA, targets are ranked from the most medial (a) to the most lateral (c) target. Mean distance (± std) between sites across subjects are indicated.

and plugged into a MagPro x100 TMS stimulator (MagVenture A/S, Denmark). The coil was robotically handled (Axilum Robotics, France) and the system was neuronavigated (Localite GmbH, Germany). Electromyography recordings were acquired using surface electrodes placed on the FDI in a tendon-belly montage plugged in a CED micro 1401 MKII recording system (Digitimer, Cambridge Electronic Design, UK). MEPs were analyzed using CortexTool to extract peak-to-peak amplitudes (Harquel et al., 2016b). The motor hotspot was defined as the target eliciting the greatest and most stable motor response. The hotspot hunting was performed on a 7x7 grid centered around the anatomical hotspot based on anatomical landmarks (Harquel et al., 2017). TMS pulses were delivered at 110% of the rMT, assessed using the threshold hunting procedure by Awiszus (2003). Stimulation intensities were adjusted for each target based on scalp-to-cortex distance using the Stokes formula (Stokes et al., 2007). The coil was positioned perpendicularly to each sulcus. 100 pulses were delivered to each target at a random frequency between 0.5-0.7 Hz. White noise was used to mask the TMS click by noise-cancelling earphones (Bose QC 20, USA). The volume was adjusted for each participant. Additionally, we performed a realistic sham condition as detailed in Raffin et al. (2020). In short, while the coil was being flipped on the placebo side, an electrical stimulation was delivered concurrently to each TMS pulse through two skin electrodes (stimulating area of 10 × 6 mm^2) placed in a bipolar montage near electrodes AF4 and F6. The electrical stimulation intensity was tuned individually for each subject, in order to mimic muscular twitches or skin sensations comparable in terms of strength, pain, or discomfort, to active TMS pulses.

2.5. EEG acquisition

EEG signals were recorded using a TMS compatible system (BrainAmp DC amplifiers and BrainCap EEG cap, Brain Products GmbH, Germany) using a cap composed of 128 passive electrodes positioned according to the 10-20 standard system. Electrode impedances were set below 5 kOhms, checked regularly during the experiment and adjusted between conditions if required. EEG signals were recorded using DC mode and digitized at 5 kHz frequency. Channels Fz and Afz served as reference and ground electrodes, respectively.

2.6. EEG preprocessing

EEG signals were processed using Fieldtrip (Oostenveld et al. (2011) according to the methods published in Rogasch et al., 2014) based on two rounds of independent component analysis (ICA), and used in our lab (Harquel et al., 2016a; Raffin et al., 2020) (Figure S1). Epoching was done around the TMS pulse on the -1 to +1 s time window of interest. TMS artifacts were cut out for the -5 to +15 ms period surrounding the pulse. By the end of the pre-processing, we removed an average of 7.4 ± 2.9 components that did not differ significantly between targets ($F_{HF}(5.4, 102.3) = 1.9$, p = 0.102; 6.3 ± 2.6, 6.9 ± 2.4 and 7.1 ± 3.4 for S1a to S1c; 7.4 ± 2.4, 7.1 ± 2.9 and 7.9 ± 2.6 for M1a to M1c; 7.7 ± 2.6, 7.9 ± 2.6 and 8.1 ± 2.6 for PMa to PMc; 8.1 ± 4.2 for realistic SHAM), and each condition comprised on average 96.2 ± 4.1 trials. Further details of the preprocessing steps can be found in Harquel et al. (2016a), Raffin et al. (2020) and Rogasch et al. (2014).

2.7. TMS evoked potentials

TEPs were computed for each target and subject by averaging the signal across trials, using baseline normalization (z-scoring) over the -200 to -5 ms period. Grand average TEPs were obtained by averaging normalized TEPs across subjects. In parallel, GMFP were obtained for each target and subject from the non-normalized TEP in Volts (see Esser et al., 2006 for the computation of such indicator). Local TEPs and single trial activity were obtained for each target, using a region of interest (ROI) defined as the 5 closest electrodes to the stimulation site. For the realistic-sham condition, local TEPs were extracted on frontal electrodes close to the site of peripheral stimulation. P30 component amplitudes were extracted from local TEPs by averaging signals between 25 and 35 ms.

In addition, local TEPs and single trial activity were computed using a common electrodes cluster gathering all ROIs. This larger cluster was used as a control for the effect of ROI definition, which could significantly influence results regarding spatial resolution. Lastly, to investigate the influence of peripheral muscle activation on the results, a second dataset containing only trials without MEPs (when possible) or the lowest MEPs was drawn from the original database and analyzed. For that purpose, 50 trials were selected based on the median split of MEPs amplitude distribution for each target and subject. When the median was equal to zero (majority of MEP negative trials), 50 trials were randomly selected. Over the entire database, most of the trials were MEP negative or induced MEPs inferior to 100 µV (51 and 62% respectively), the latter being of 47% and 69% on M1 and non-M1 targets respectively.

2.8. Regression quality scores

Regression quality scores were computed using the method presented in Raffin et al. (2020). Different linear regression analyses were performed at the scalp level. First, as described above, the local TEPs $x_i(t)$ were derived for each grid point i, each trial k (from 1 to n trials), and each subject, from +15 to +80 ms, in order to exclusively encompass the early components of the evoked activity. Then, linear regressions of the local TEPs $x_i(t)$ were performed for each grid point i on single trials $s_{jk}(t)$ extracted from each grid point j and trial k, so that:

$$s_{jk}(t) = \beta_{ijk} * x_i(t) + \varepsilon(t), t \in [15, 80]\text{ms},$$
$$\text{with}(i, j) \in \{S1a, S1b, S1c, M1a, M1b, M1c, PMa, PMb, PMc, sham\}$$

The quality of the linear regression was then assessed by extracting t-statistics associated to the local TEP x_i factor for each trial, grid point and subject, and finally averaged across trials to obtain RQS for each grid point pair and subject. Specifically, β_{ijk} is given by:

$$\beta_{ijk} = \frac{\sum_t \left(x_i(t) \times s_{jk}(t)\right)}{\sum_t \left(x_i(t)^2 - \bar{x}_i^2\right)}$$

Each β_{ijk} is studentized (centered and reduced) to obtain a t_{ijk} statistics. Finally, RQS are the mean of the t statistics across trials for each subject:

$$RQS_{ij} = \frac{1}{n}\sum_{k=1}^{n} t_{ijk}$$

The term "paired sites" (pRQS), used throughout this manuscript, refers to pairs where $i=j$, i.e. where the regressed TEP x_i and single trials s_j are taken from the same grid point, also referred as *local regression*. Analyzing such local regressions *via* RQS on paired sites allows assessing the cortical excitability level of a particular grid point *i* (Raffin et al., 2020). At similar stimulation intensities, the higher the RQS on site *i*, the higher the level of cortical excitability of site *i* is. This is based on the hypothesis that the electrical activity produced by highly excitable neural populations would be more differentiable from noise, and moreover more frequently, than the one produced by low-excitable ones.

In addition, the term "unpaired sites" (uRQS) refers to pairs where $i \neq j$, *i.e.* where the TEP x_i computed on grid point *i* is regressed on single trials of another grid point *j*, also referred as *remote regression*. Analyzing such remote regressions *via* RQS on unpaired sites allows assessing the level of similarity between the response dynamics of grid point *i* and *j*. The higher the RQS between sites *i* and *j*, the higher the match in response dynamics between sites *i* and *j* is. For display purpose, grand average RQS were plotted over the cortical surface segmented from a brain template (Tadel et al., 2011).

2.9. Induced electrical field modelling

Electric field estimations were computed based on the finite element method, using individualized head meshes based on each participant T1w MRI (Thielscher et al., 2015). Head reconstructions were performed using the *headreco* pipeline (Nielsen et al., 2018). Using the SimNibs 3.2 Graphical Interface, we then placed each target of the grid relative to its exact position on the neuronavigation system. The MagVenture B70 template included in SimNibs was used for the simulations, the di/dt being adjusted for each target. For each contrast (e.g. M1-S1, or b-a), the three field strengths related to the tested positions were averaged prior to computing the difference (e.g. M1-S1 = (M1a + M1b + M1c) / 3 - (S1a + S1b + S1c) / 3, or b-a = (S1b + M1b + PMb) / 3 - (S1a + M1a + PMa) / 3).

2.10. Statistical analysis

Statistical analyses were conducted with Fieldtrip (Oostenveld et al., 2011), Rstudio and Jamovi (*RStudio Team (2019). RStudio: Integrated Development for R. RStudio, Inc., Boston, MA URL* http://www.rstudio.com/., n.d.; *The jamovi project (2020). jamovi (Version 1.2) [Computer Software]. Retrieved from* https://www.jamovi.org, n.d.), and are detailed thereafter. For repeated measure ANOVA (rmANOVA), whenever the assumption of sphericity was violated (Mauchly's test, $p < 0.05$), a Huynh-Feldt correction was applied, and the subsequent F values were reported as F_{HF} together with the corrected degrees of freedom. All *post-hoc* tests subsequent to ANOVA-like models, as well as multiple comparison or correlation tests, were Bonferroni corrected and reported as p_{bonf}.

At a global level, evoked electrical field topographies were compared between all conditions using cluster-based permutation tests at the scalp level (using Fieldtrip's *ft_timelock* statistic function, with "Monte-Carlo" and "cluster" as main parameters). A dependent multivariate F-test was applied at sample level on all electrodes in order to draw clusters of at least 2 neighboring channels under the significance threshold of $\alpha = 0.05$. Both early and late components were tested using a [15, 80] and [80, 400] ms time window respectively. Cluster-level statistics were thereafter computed by summing the *F*-values within each cluster and Monte-Carlo procedure (1,000 permutations) was used for correction. Clusters were considered significant under the significance threshold of $p_{cluster} < 0.05$.

Local regressions (pRQS) were analyzed using rmANOVA across subjects, with two fixed effects: Brodmann area (S1, M1 and PM) and mediolateral position of the targets (a, b and c). Local regressions were compared to two other metrics (P30 component amplitude and MEP amplitude) using Spearman correlation. To account for the spatial correlation in the analysis of remote regressions (uRQS), we used the spam package (https://cran.r-project.org/web/packages/spaMM/) that implement spatial Generalized Mixed Models (spaGLMMs, (Rousset and Ferdy, 2014)). Spatial autocorrelations were fitted by Gaussian process as well as random term and fixed effects were evaluated using a model comparison procedure, i.e. removing a factor from a model and comparing the fit and residual errors. Since RQS distributions were left skewed, we used a square root transformation on data and checked for normality prior to the modeling of fixed and random effects. We run this analysis using the same two fixed effects, *i.e.* BA and mediolateral position of the targets, and two random effects: subjects and spatial random effect (distance between x_i and s_j).

The maximum values of the induced E-field strength were compared between targets by means of an rmANOVA across subjects, with the same two fixed effects previously described (BA and mediolateral position). Then, the relationship between these maxima and pRQS was explored using Spearman correlation. The E-field contrasts between BAs and mediolateral positions were analyzed using an ANCOVA. The maximum of the absolute contrasts between E-field strength (see section 2.9) was entered as the dependent variable, while the direction (either across BA or along the mediolateral direction) and the mean distance between targets (in mm) were defined as fixed factor and covariate respectively. Lastly, the link between uRQS and these maxima was analyzed using the same statistical model, with the mean uRQS (across BA or mediolateral axis) as the dependent variable and the absolute contrasts between E-field as a covariate.

3. Results

3.1. Global evoked activity

The global evoked activity of each cortical target is showed by means of GMFP and current topographies in Figure 2.A and 2.B respectively. Overall, the displacement of the stimulation over the grid evoked different patterns of response at a global scale, both on the BA and the mediolateral directions. Cluster-based permutation tests revealed a significant difference across position on induced responses in both early and late components windows ($p_{cluster} < 0.05$). The difference was most pronounced during the 35 to 50 ms and 104 to 181 ms periods for early and late components respectively. Realistic sham condition induced important responses (> 2 σ from baseline) during the late time window starting from 80 ms.

3.2. Local TEPs

Figure 3.A shows the local evoked response to TMS regarding each BA and each lateral position. Additionally, each plot displays the active sham TEP for the frontal electrodes closest to the electric stimulation. The local activities exhibit patterns that seems specific to each area and modulated by the position along the mediolateral axis. This qualitative observation made on group-averaged signal is explored thoroughly in the following sections.

3.3. Local regression

The first analysis of the study relied on local regressions using paired RQS (pRQS) (Raffin et al., 2020), which is a way to quantify both the SNR ratio and inter-trial variability (response stability), which has been related to the cortical excitability level. Figure 3.B.1 gives examples of the calculated pRQS in each site for two representative subjects, while depicting the local early TEPs and its corresponding individual trials matrices. The individual TEPs illustrate the inter-individual variability in evoked dynamics, the components varying in terms of number, relative amplitude and latency (see also Figure 3.B.2). Conditions presenting the largest and more stable activities across trials got the highest pRQS

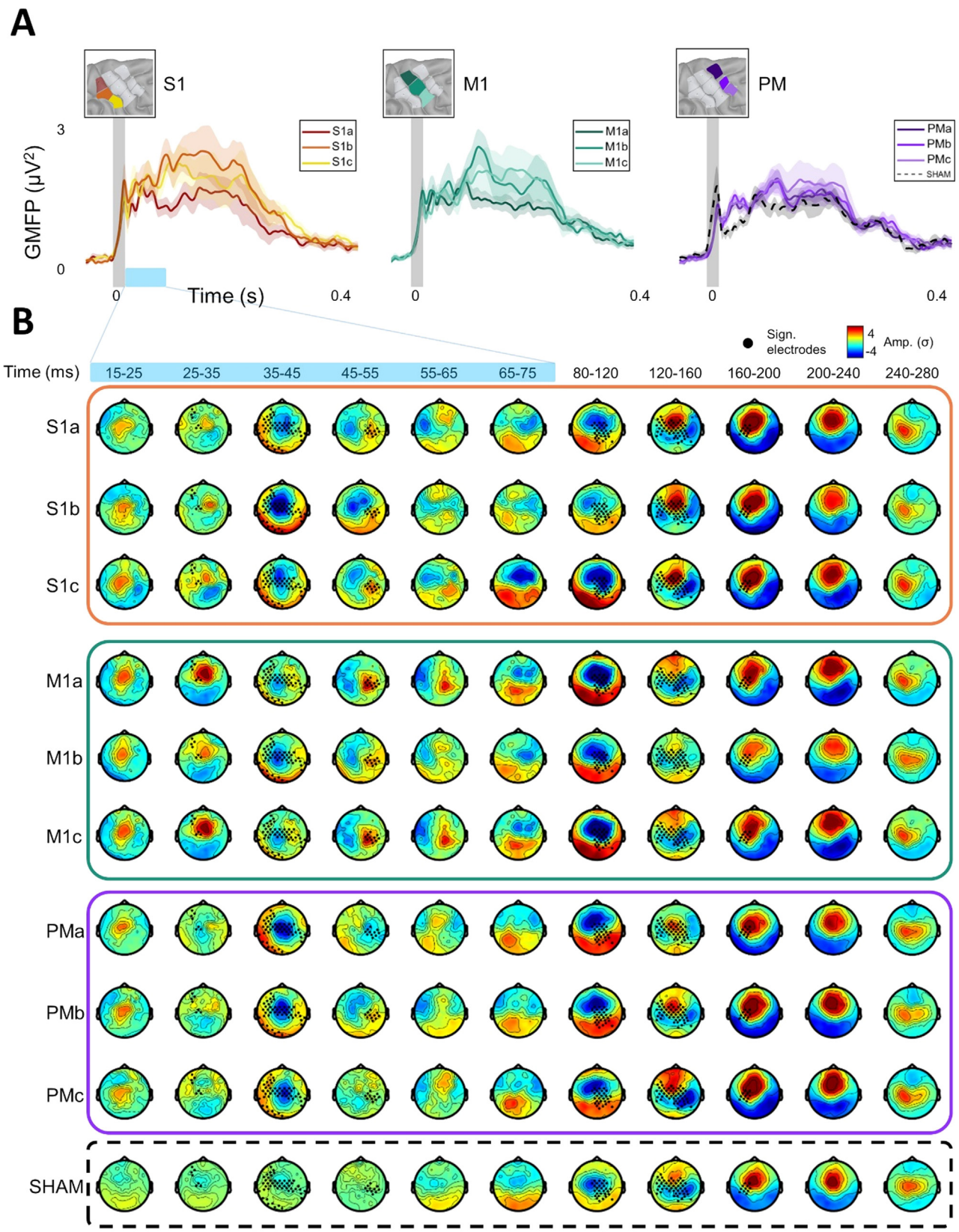

Fig. 2. - Global evoked activity. A. Grand average global mean field power (GMFP) for each target, sorted from posterior to anterior positions (from left to right). Colors code for laterality of the site, the darker the more medial. Colored shaded areas indicate the 95% confidence interval for each GMFP. Grey shaded areas indicate the -5 to +15 ms TMS pulse interpolation period. B. Grand average topographies for each target, sorted from posterior to anterior and from medial to lateral positions (from top to bottom). The six first topographies highlighted in cyan span the early evoked activities from 15 to 80 ms using a 10 ms step, the five last spanning the late evoked activities using a 40 ms step. Electrodes belonging to a significant cluster (as measured by cluster-based permutation tests, see section 2.10) for at least one sample within the plotted period are highlighted with black dots.

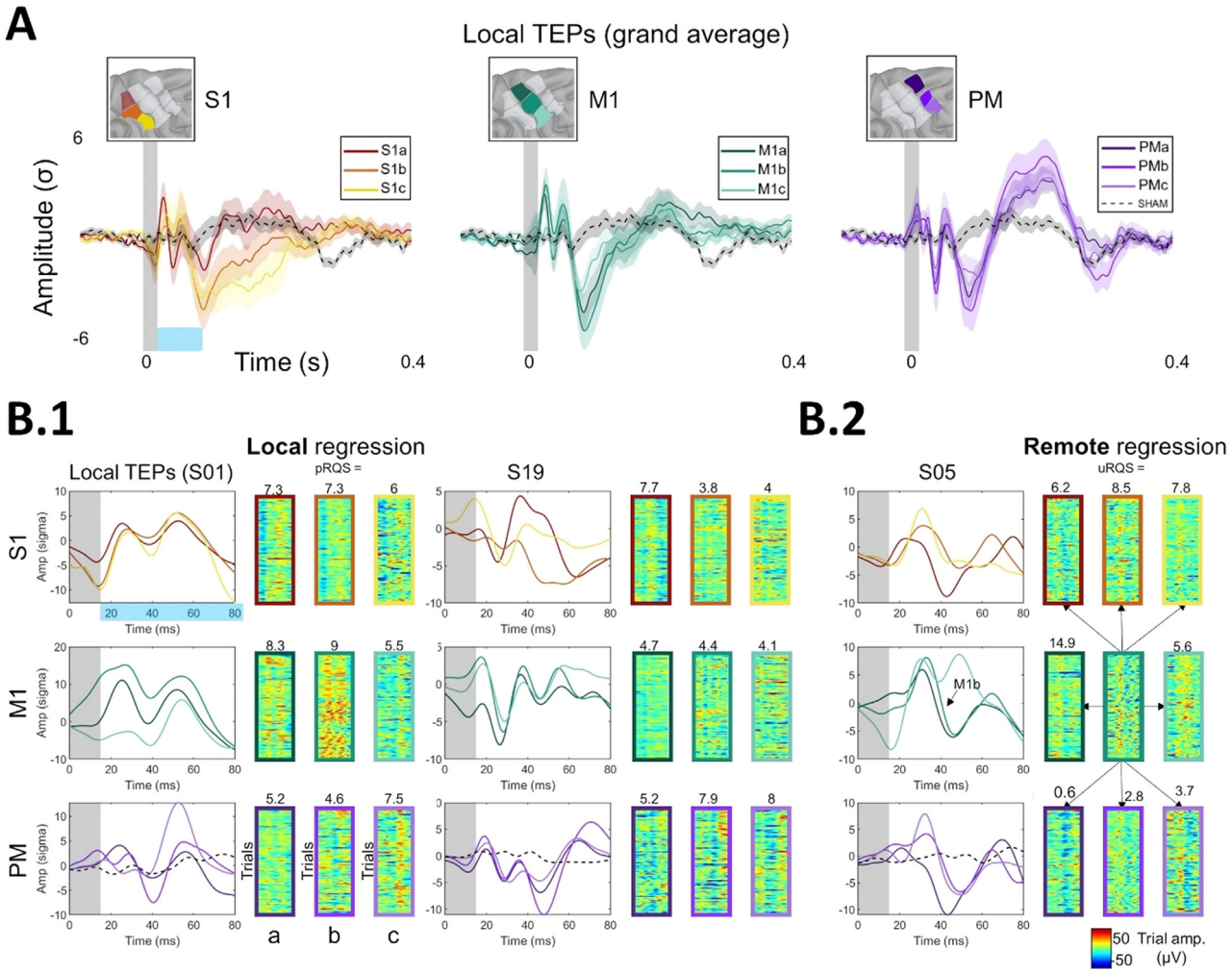

Fig. 3. - Grand average and individual local TEPs. A. Grand average local TEPs, sorted from posterior to anterior sites (left to right). Amplitudes are displayed in standard deviation to the mean (± 95% CI). Colors code for laterality of the site, the darker the more medial. B. Early components (15-80 ms) of individual local TEPs (left) and single trials with their mean RQS value (right) from three representative subjects. B.1. Examples of local regression scores (paired RQS) computed for each target. B.2. Examples of remote regression scores (unpaired RQS) computed for each target using M1b as the reference TEP (see section 2.8).

values (see e.g. M1b or S1a for S01, and PMb/c or S1a for S19). In opposite, other sites are penalized with a low pRQS value because of unstable response (see e.g. M1c for S01, and S1b or M1a for S19), despite presenting components that differed from baseline and were comparable in terms of amplitude with the sites presenting higher RQS on TEP level.

Group results on local regressions are displayed on a brain map in Figure 4.A, next to the mean amplitude of P30 component and the mean MEP amplitude of FDI muscle for comparison. First, pRQS of active stimulation differed significantly from realistic sham for all conditions (paired t-tests, all $p_{bonf} < 0.05$). The paired RQS was 3.07 ± 1.84 for realistic sham, which was concordant with our previous findings (Raffin et al., 2020). Then, the rmANOVA analysis showed that pRQS differed significantly across BA ($F(2,38) = 4.12$, $p = 0.024$), while no effect of the position along the mediolateral axis of the target, and no interaction between the position along the mediolateral axis and BA stimulated were found. *Post-hoc* analyses between BA revealed that RQS were significantly higher in S1 than in PM ($p_{bonf} = 0.014$), while no difference were found between S1 and M1, nor between M1 and PM. Regarding MEP, we found a significant effect for the BA factor ($F(2,38) = 16.6$, $p < 0.001$), the positioning factor ($F(2,38) = 4.2$, $p = 0.022$), and their interaction ($F(4,76) = 4$, $p = 0.005$). *Post-hoc* tests revealed that M1 differed significantly from S1 and PM ($p_{bonf} < 0.001$) while no difference was found between S1 and PM. Lastly, the P30 component solely differed significantly across BA ($F(2,38) = 18.8$, $p < 0.001$), where every *post-hoc* comparisons showed significant differences (M1 vs. PM, $p_{bonf} < 0.001$; M1 vs. S1, $p_{bonf} = 0.026$; S1 vs. PM, $p_{bonf} = 0.012$).

Comparisons between local regression and the two other metrics (Figure 4.B) showed a significant correlation between paired RQS and P30 component amplitude (Spearman's $\rho = [0.11\ 0.38]_{95\%CI}$, $p_{bonf} < 0.001$), but not between paired RQS and MEP amplitude ($\rho = [-0.01\ 0.27]_{95\%CI}$, $p_{bonf} = 0.230$). Lastly, a significant correlation was found between P30 component and MEP amplitudes (Figure 4.C, $\rho = [0.09\ 0.37]_{95\%CI}$, $p_{bonf} = 0.003$).

3.4. Remote regression

The second analysis relied on remote regressions using unpaired RQS (uRQS) (Raffin et al., 2020), which quantifies the similarities in evoked dynamics between sites. This indicator is illustrated in Figure 3.B.2, where examples of the calculated uRQS from M1b (reference TEP) towards each other site are given for one representative subject, together with the local early TEPs and its corresponding individual trials matrices. Sites presenting trials in which the evoked dynamics are consistently close to the reference site got the highest remote regression scores (see e.g. M1a and S1b), while these latter are dropping when dynamics across sites are diverging (see e.g. PMa).

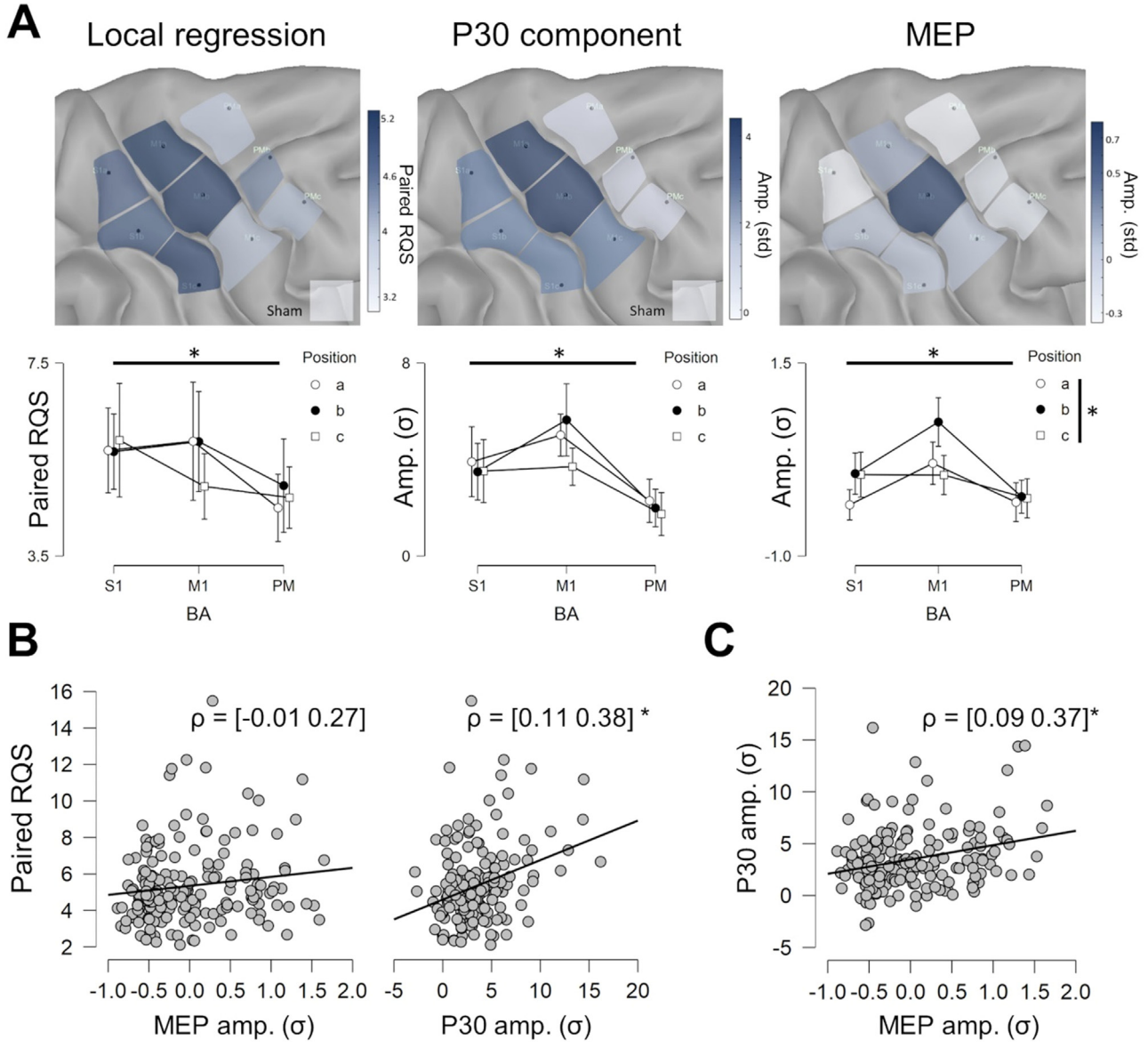

Fig. 4. – Local regression and comparison with P30 component and FDI's MEP. A. Maps (top) and data distributions (bottom) of local regression, P30 component of local TEP and FDI's MEP on the nine targets and sham condition (from left to right). Stars denote significant effect of the main factors of the rmANOVA, i.e. BA and mediolateral axis position. B. Correlation between local regression and FDI's MEP (left), and P30 component (right). C. Correlation between P30 component and FDI's MEP.

Overall, we found RQS were higher when the reference TEP was processed with local regression compared to remote regressions, in which RQS are decreasing with distance to the reference site (Figure 5), before eventually reaching noise level. Noise level (uRQS = 1.10) was defined as the mean uRQS computed by taking sham local TEP as a reference signal for the regressions. Using a generalized mixed model analysis accounting for spatial correlation, we compared three factors representing our three hypotheses regarding this decrease (Figure 6). First, we found a significant effect of the distance from stimulation site (x_i) to the target (s_j) ($\chi^2(1) = 356.28, p < 0.001$) captured by spatial random effect, and a significant effect regarding the stimulated BA ($\chi^2(2) = 14.88, p < 0.001$). No effect was found for the position along the mediolateral axis ($\chi^2(2) = 5.62, p = 0.06$) and no interaction between stimulated BA and position along the mediolateral axis ($\chi^2(4) = 2.14, p = 0.71$).

Finally, these results were not modulated by the use of a common electrodes group gathering all ROIs, or by only selecting trials inducing the lowest MEPs (see section 2.7). When computing RQS using a common ROI, the spatial random effect was still significant ($\chi^2(1) = 108.68, p < 0.001$), as well as the stimulated BA factor ($\chi^2(2) = 52.37, p < 0.001$). Applying the model on trials inducing the lowest MEPs also revealed a significant effect of the spatial distance from stimulation site to the target ($\chi^2(1) = 167.14, p < 0.001$), and a significant effect regarding the stimulated BA ($\chi^2(2) = 21.01, p < 0.001$). For both models, no effect was found for the position along the mediolateral axis and its interaction with BA.

3.5. Modulation of remote regression by distance

We studied more specifically how RQS varies according to distance from the reference TEP (Figure 7). Overall, the RQS were significantly decreasing with respect to this distance using all data (Kendall's τ = -0.2, p < 1 e-35), 15 subjects over 20 showing this effect using individual data ($p_{bonf} < 0.05$). RQS were dropping at 50% of their values between 25 and 30 mm from the reference site, and they became similar to paired and unpaired sham RQS at a distance of 10 and 40 mm respectively.

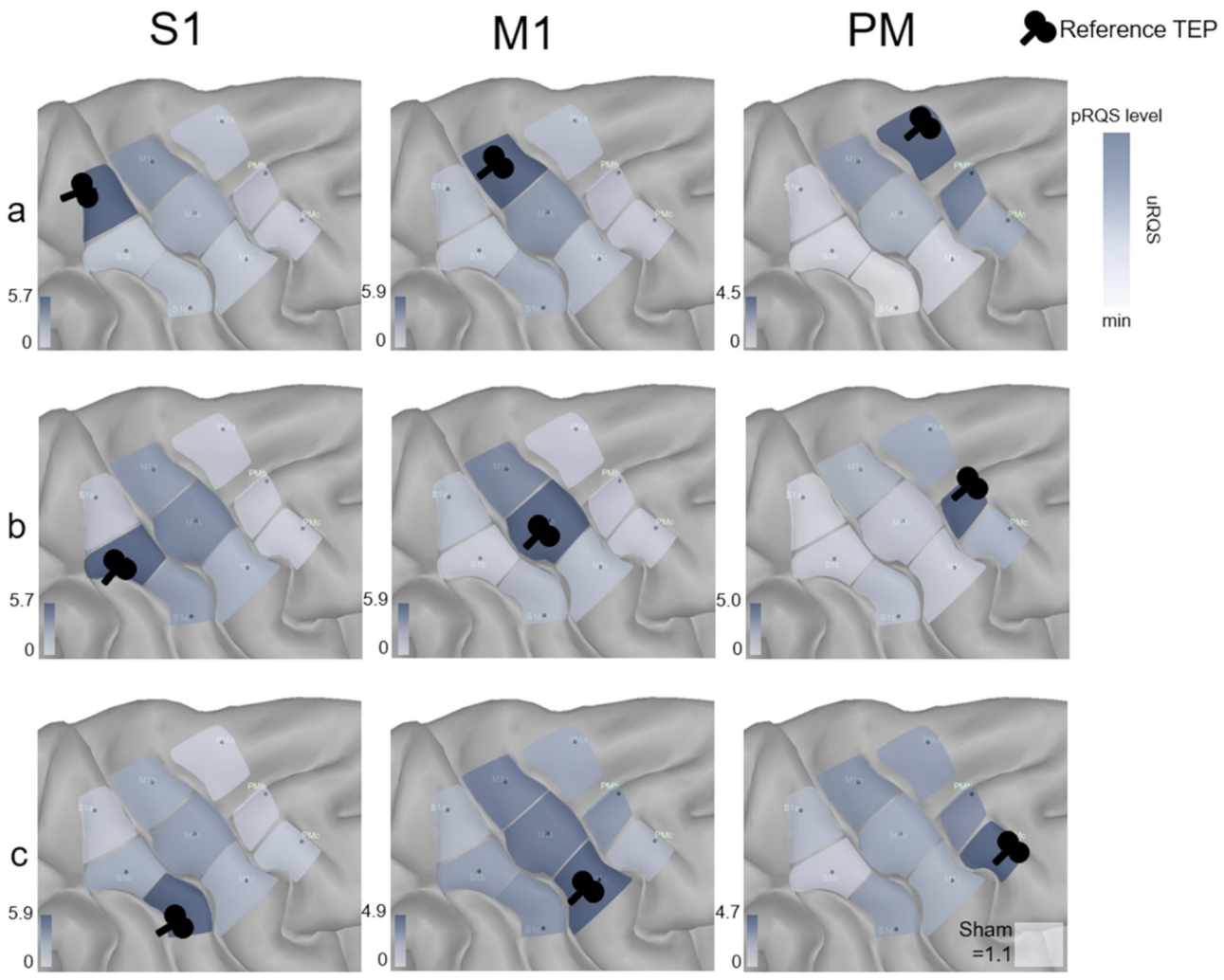

Fig. 5. - Maps of remote regressions on the nine targets and sham condition. Each map represents the remote regression of one particular site by showing the corresponding unpaired RQS. A coil drawing indicates the site taken for the reference TEP $x_i(t)$. The reference TEPs used for the regressions are sorted from posterior to anterior, and from the most medial to the most lateral targets, on the X and Y axes respectively. Note that local regressions consist of using the reference TEP in its proper target, which correspond to the maximum RQS on each of the 9 maps.

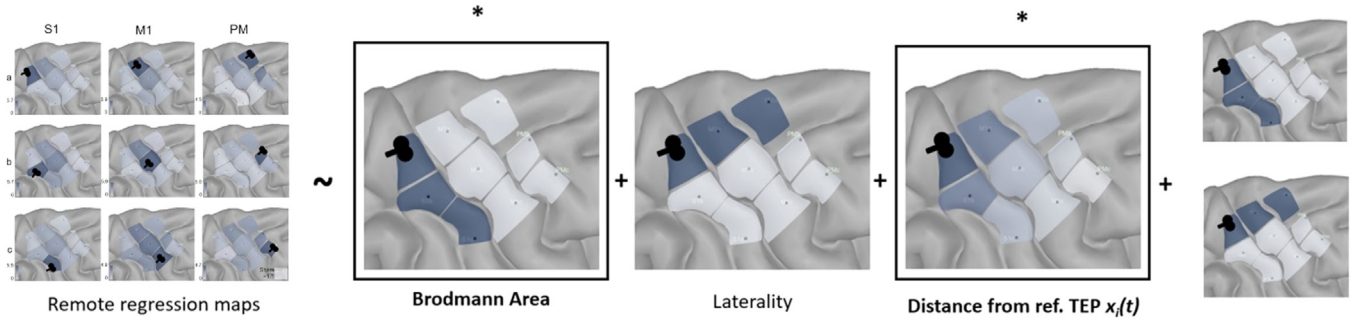

Fig. 6. - Graphical representation of the spatial linear mixed model's results on remote regression (see section 3.4), showing a significant effect of both BA and distance from the reference TEP factors (1st and 3rd respectively). The colorbar is identical to the one used in Figure 5.

Analyzed separately, all the sites showed a significant decrease (τ ranged from -0.1 to -0.3, $p_{bonf} < 0.05$ to $p_{bonf} <$ 1e-8).

3.6. Link with induced electrical field modeling

Finally, the induced electrical field was estimated for each cortical target and subject. Figure 8.A.1 shows the resulting distribution of the electrical field strength for two representative subjects. If the spatial distributions were overlapping between targets, it was still possible to note a displacement of the field, especially along the antero-posterior direction (i.e. between different BA). In addition, the maximum of the induced electrical field significantly differed across both BA (rmANOVA, $F_{HF}(1.5, 28) = 11.81$, $p < 0.001$) and position along the medio-lateral

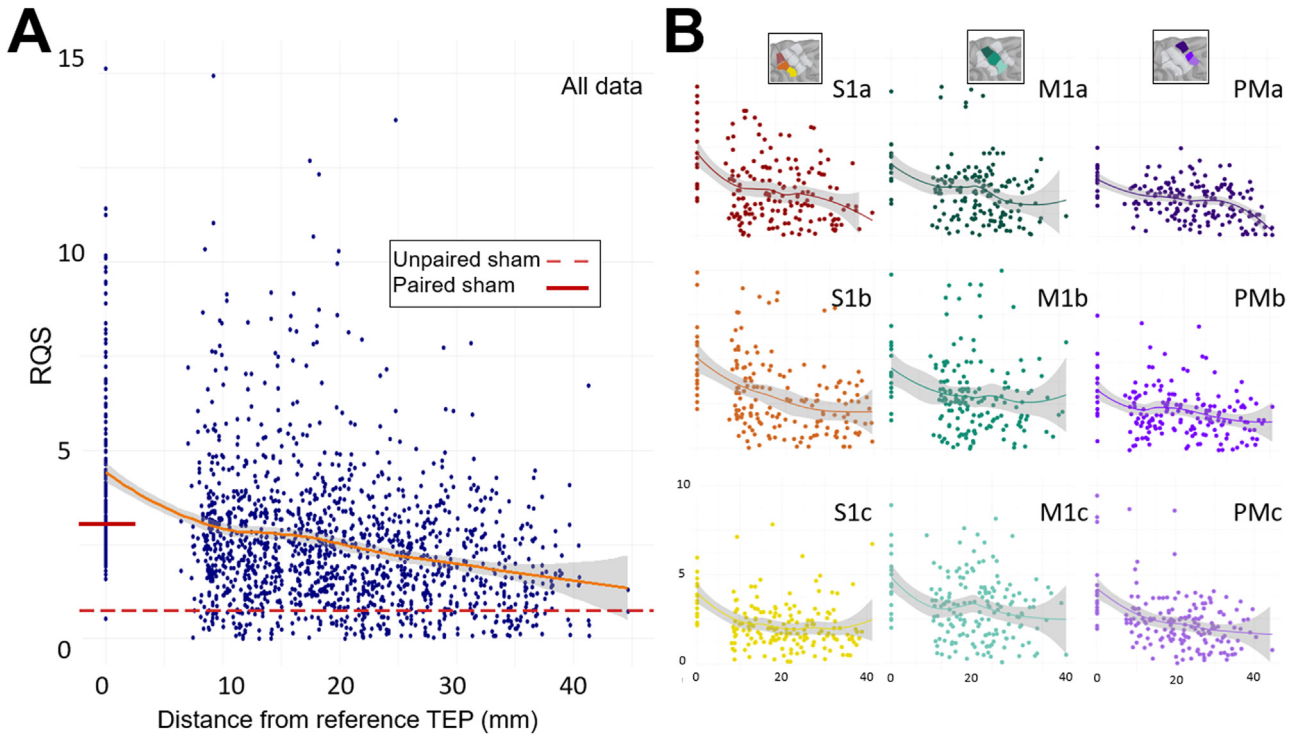

Fig. 7. - Distribution of RQS in relation to distance from the reference site, for all subjects and stimulation sites (panel A), and grouped by each stimulation site (panel B). Trends are a fit to the mean ±95% CI. Mean paired and unpaired RQS obtained with sham condition are indicated in panel A.

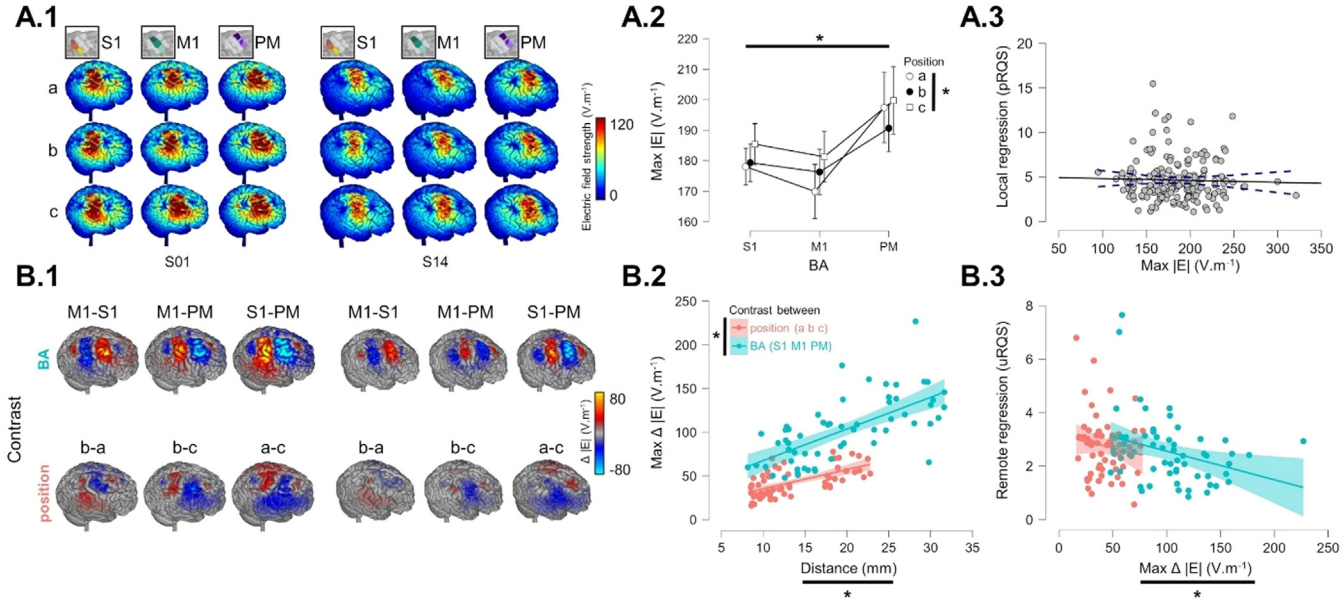

Fig. 8. - Relationship with TMS induced E-field modelling. A.1. Examples of induced E-field strength (|E|) computed on each target for two representative subjects. A.2. Data distribution of the maximum of E-field strength across BAs and mediolateral positions. A.3. Local regression scores (pRQS) as a function of the maximum of E-field strength. B.1. Contrasts of E-field strength spatial distribution along BA (top) and mediolateral (bottom) direction. For each contrast, the three fields related to the tested positions were averaged prior to computing the difference (see section 2.9). B.2. Distribution of the maximum of the absolute contrast between E-field strength in function of the distance and the contrast direction. B.3. Remote regression scores (uRQS) as a function of the maximum of the absolute contrast between E-field strength, grouped by contrast direction. For each plot, stars denote significant effect of the corresponding main factor.

axis (F_{HF}(1.9, 36.6) = 3.79, p = 0.033), the interaction between these two factors being non-significant (F_{HF}(2.8, 52.9) = 0.96, p = 0.414) (Figure 8..A.2). The premotor and most lateral position where the targets on which the field presented its strongest peak. However, we did not find any correlation between the maximum of this field and the corresponding local regression values (ρ = [-0.17 0.12], p = 0.691, Figure 8.A.3).

Secondly, we studied the difference in induced field strength depending on whether the displacement was made on the anteroposterior (i.e. across BA, from S1 to PM) or on the mediolateral axes (from position

a to c). Figure 8.B.1 shows the resulting contrasts for the same above subjects. If the contrasts across BA revealed results in accordance with the underlying experimental hypothesis (e.g., when selected as a target, S1 is more stimulated than M1 or PM, Figure 8.B.1, top row), this link was less clear on the mediolateral axes (bottom row). These contrasts revealed more complex spatial patterns, the comparison between the most distal points (a-c) showing the more consistent results. Moreover, it was observed that the contrasts were systematically stronger on the anteroposterior axis than on the mediolateral one. Figure 8.B.2 details this aspect, by showing the absolute maximum of the contrasts between E-field strength in function of the distance between targets, and the direction of the contrast (either along BA or mediolateral direction). The ANCOVA showed a significant effect of distance ($F(1, 98) = 132.3$, $p < 0.001$), the greater the distance between targets the greater the difference in E-field strength, and a significant effect of contrast direction ($F(1, 98) = 122.89$, $p < 0.001$). The latter underlies an interesting anisotropic relationship: whatever the distance between contrasted targets, the difference of E-field strength was greater when contrasting between BA than between mediolateral axis. Finally, applied to uRQS, the ANCOVA revealed a significant link with the difference of E-field strength ($F(1, 98) = 10.64$, $p = 0.002$), while no effect was found for the contrast direction ($F(1, 98) = 2.95$, $p = 0.089$).

4. Discussion

In this study, we tried to assess the spatial resolution of TMS-EEG on the sensorimotor system, using RQS of both local and remote regressions of early components of TEPs as a metric. First, we showed that this metric was a useful tool for mapping cortical excitability of the sensorimotor area, which might be less prone to peripheral confounds compared to other classical EEG and EMG metrics. Then, we found that the neighboring stimulation targets distant from 10 to 15 mm on the stimulation grid evoked a specific response that could be significantly differentiated, even though the dynamical signature of a specific site can be found in its neighborhood up to 25-30 mm, most particularly between sites within the same BA. These experimental results were also in line with the predictions made by E-field modeling. Finally, we found that laterality did not evoke specific dynamic patterns, suggesting that PEPs may not have significant impact on the composition of early components of TEPs.

4.1. Cortical excitability

Considering local regression scores (paired RQS) as a marker of local cortical excitability, we found that this latter was significantly modulated across Brodmann areas. The rationale supporting this idea is that, at a similar stimulation intensity, highly excitable population would tend to produce a stronger (better signal-over-noise ratio increases pRQS) and more stable (lower inter-trial variability increases pRQS) activity than low-excitable populations (Raffin et al., 2020). The main advantage of this technique is to handle both inter and intra-subject variability regarding the evoked neural response dynamics (Bridwell et al., 2018). Consequently, it has to be noted that the use of this readout does not allow to draw finer conclusion, especially on the modulation of specific evoked components seen at the group level within a particular cortical area (e.g. the N45 of M1), which are linked to different underlying neural mechanisms (e.g. the inhibitory GABAergic system, see Darmani and Ziemann, 2019 for a recent review of pharmacological TMS-EEG studies).

The largest excitability of the primary motor and sensory areas compared to the premotor cortex is in line with previous results comparing M1 to other cortical areas in the frontal or occipital lobes (Fecchio et al., 2017; Harquel et al., 2016a; Raffin et al., 2020). Moreover, mapping the P30 amplitude led to a sharp map presenting a unique maximum over the motor hotspot, that was significantly correlated with corresponding motor mapping using EMG (Figure 4.C). As such, P30 could be correlated with the activation of the corticospinal tract inducing muscular contraction and might be not relevant for exploring cortical excitability of areas outside M1, and even outside a targeted motor hotspot. This might also be the case for any other components, as their electrophysiological nature varies from one site to another, essentially as a result of the cytoarchitectonics differences observed throughout the cortex (Harquel et al., 2016a). By considering the full dynamics of the evoked signal over each individual, site, and trial, local regression scores would be more informative than any other measure based on a sole evoked component and would allow for direct comparison between sites.

Despite Stokes correction, significant differences in the maximum induced E-field strength were observed across BAs and positions (Figure 8.A.2, in accordance with the previous findings of (Janssen et al., 2014; Konakanchi et al., 2020)), which could somehow bias the original hypothesis regarding uniform stimulation intensity. As such, the excitability of premotor areas might even be lower than measured here, given the fact that the induced fields were stronger when stimulating these sites. However, local regression values (pRQS) were not correlated with the computed maximum E-field strength (Figure 8..A.3), which gives rise to two mutually non-exclusive interpretations. First, the single trial stability and strength as measured by pRQS does not solely depends on the stimulation intensity, but rather on a complex interaction between several and biophysical parameters including cytoarchitectonic, myelin content, or different temporal dynamics of the E-field waveform (e.g., pulse shape width, current direction, or phase amplitude asymmetry) (Aberra et al., 2020). Second, this field's feature (maximum strength) might not be the best indicator for depicting the true stimulation intensity, compared to more integrated measures like spatial spread or the exact concordance between induced field and axon directions for each site (Aberra et al., 2020).

4.2. Spatial resolution of TMS-EEG coupling

The significant contribution of the spatial random effect found within the analysis on remote regressions showed that the TMS evoked dynamics were significantly specific to each site (Figure 5 & 6). As such, the spatial resolution of TMS-EEG coupling might be fine enough to distinguish sites separated at least from 10 to 15 mm, which was the mean range of distances between sites in this study. This promising result suggests that TMS-EEG coupling benefits both from the spatial resolution of TMS, which can be as high as 5-7 mm when considering results obtained with EMG markers over M1 (see e.g. Harquel et al., 2017), and the temporal resolution of EEG. The relatively low spatial resolution of scalp EEG, which is estimated to be around 5 to 9 cm (Burle et al., 2015) principally due to current spreading and volume conduction, would not be significant when considering the resolution of the TMS-EEG coupling as a whole. Interestingly, the somehow discrepancy found between the large spatial spreading predicted by E-field modeling (Figure 8.A.1) and the actual measured resolution using EEG (or other behavioral or electrophysiological outcomes like EMG) is in line with a recent study using single-neuron recordings in macaque (Romero et al., 2019). Even if animal to human translation is not straightforward, their results suggest that the focality of the TMS aftereffects on neural activity might be ten time higher than expected by E-field simulations. Overall, these findings are highly relevant when designing TMS-EEG mapping grids, especially for clinical applications.

However, shared dynamics and temporal EEG signal properties can be found in neighboring sites distant up to 25-30 mm (Figure 7). These results can partly be explained by the current spread of the induced electrical field on the cortex, and therefore its spread to neighboring areas (see Figure 8 and (Bungert et al., 2017; Opitz et al., 2011; Thielscher et al., 2015)). TMS pulses induce depolarization of local neuronal populations, leading to a specific dynamic of response due to the unicity of both anatomical and functional characteristics of the stimulated site. It also activates some neighboring populations of neurons, which will then add a trace of their specific dynamic onto the response, decaying with the relative distance from the stimulation site. Interest-

ingly, this decrease was somehow predicted by the induced E-field modelling, where the differences in dynamics negatively correlated with the contrast strength between fields (Figure 8..B.3). Our results would then prove that, below 25-30 mm, the evoked dynamic properties of two neighboring sites are somehow overlapping. This limitation could be overcome with the improvement of TMS coils (Colella et al., 2019) and the *a priori* optimization of its position using the TMS inverse problem approach (Makarov et al., 2021), allowing for a better focality of the induced electrical field. It would also be interesting to test spatial resolution using lower stimulation intensities, for which the induced electrical current spread is smaller. Another way to overcome this limitation would be to extract neural activity from the targeted populations at shorter latencies (Veniero et al., 2013), which would be even less prone to be affected by common effective connectivity from remote cortical and non-cortical sites.

We also found that these similarities regarding evoked dynamics were more significant between sites within the same BA, remote regressions being higher when the reference TEP was taken from the same BA (Figure 5 & 6). This result suggests an anisotropic spatial resolution that would be higher across than within BA, as the cytoarchitectonics of the stimulated area plays an important role in the TEP's composition (Harquel et al., 2016a). However, two arguments might lower this statement. First, the interval of the distances covered across BA direction was greater than that covered across the mediolateral axis at the group level. More importantly, the E-field modelling also predicted this anisotropy. Even at a similar distance (between 7 and 23 mm), the difference in induced E-field strength between two targets was significantly stronger between than within BA (Figure 8.B.2). This could be explained by anatomical factors, where crossing a gyrus border would have a stronger impact on the final spatial distribution of the induced field than following it (Janssen et al., 2014). Finally, the cytoarchitecture of both M1 and S1 being very similar along their gyrus, the extension of this result to other gyri or Brodmann areas might be not straightforward (Heuvel et al., 2015). Still, remote regressions could be used in future studies to functionally define a cortical area of interest, by mapping the reference TEP of its center; the boundaries of the defined area being the targets where RQS falls below noise level.

A future development for exploring TMS-EEG spatial resolution might be to use finer stimulation grid in line with TMS motor mapping studies (Harquel et al., 2017; Meincke et al., 2016; Reijonen et al., 2020), since our conclusion is limited by the spatial resolution of the stimulation grid itself, with the actual spatial resolution of the technique possibly being even lower. Another line of direction would be to perform the same TMS-EEG mapping study using monophasic single pulses. The present approach used biphasic pulses in order to minimize stimulation intensities and therefore improve data quality but might have hampered neuronal selectivity and spatial resolution (Aberra et al., 2020).

4.3. Influence of PEPs

Lastly, we considered the influence of PEPs on the regression method, and indirectly on the early components of the evoked response. If we take into account the sensory evoked potential induced by scalp muscle contraction, TEPs should be partially composed of PEPs, especially for the most lateral sites where muscles are more implanted (Mutanen et al., 2013). Therefore, we should find a common dynamical signature between sites situated on the same mediolateral position, as the sensory evoked potentials are somehow stereotypical. However, we did not find any effect of the mediolateral position, suggesting that PEPs play a non-significant role in RQS calculation compared to the neural response directly induced by TMS. This has not to be taken as a definitive conclusion, as the width of the area stimulated may have been too narrow relatively to the mediolateral axis. The difference in muscle implantation underneath the coil from the most medial to the most lateral targets of our grid may not be sufficient to significantly elicit different PEPs (Figure S1). Finally, one experimental way to control for this aspect would have been to quantify the perception of stimulation on subjective scales for each subject, and test whether or not it was different between targets (Conde et al., 2018).

Furthermore, PEPs also cover the reafferent somatosensory activity from muscle movements. First, despite covering latencies potentially affected by this reafference (> 40 ms), local regressions (pRQS) seem to be insensitive to this contamination since the resulting functional maps were not correlated with motor maps using EMG as readouts (Figure 4.B). Furthermore, the influence of sensorimotor activations on the main result of this work appears to be marginal, since the results on remote regression (uRQS) were not modulated by the presence or absence of MEPs, or the presence of high or low MEPs amplitude within the trials dataset. These results can be interpreted in the context of the current debate on the origin of the TMS evoked potential (Belardinelli et al., 2019; Conde et al., 2018; Siebner et al., 2019). Our results are rather in line with recent results in the literature showing little to no influence of PEPs on the early components of the TEP (Biabani et al., 2019; Freedberg et al., 2020; Raffin et al., 2020).

4.4. Limitations

First, the scalp level analysis framework chosen here might have been suboptimal for assessing spatial resolution. If local TEPs is a widely used readout since TMS-EEG coupling gains from very strong *a priori* on the location of the activated cortical area at t=0 (Tremblay et al., 2019) analyzing the signal in source space might have improved the results by getting rid of volume conduction effect (Baillet et al., 2001). However, since our results were not modulated by the choice of the ROI size and centering, the observed differentiations could instead be mainly supported by the intrinsic dynamics of the signal in the time domain. Lastly, the early components of TEPs (under 100 ms) are very sensitive to the EEG signal preprocessing methodology (Bertazzoli et al., 2021), and this latter might have influenced our findings about spatial resolution. We chose to apply the two round ICA method, that has been extensively validated in the past (Bertazzoli et al., 2021; Rogasch et al., 2017), but a generalization of this results to other preprocessing methods would be yet to be done. Overall, the intra-subject variability of the preprocessing efficiency within the stimulation grid had little influence on our results, given the fact that the raw datasets noise level was uniformly distributed and equally corrected across targets (Figure S1).

Another limitation of this study lies on the stimulation intensity chosen. We stimulated at a fixed intensity corrected for scalp-to-cortex distances. However, other mapping approach could have been considered. In motor mapping setting, one could use a mapping of rMT at different targets to assess the muscle specificity of the target (Meincke et al., 2016). For TMS-EEG, we could consider using the rt-TEP toolbox to determine the optimal stimulation intensity at each site (Casarotto et al., 2022). However, the choice of the TEP feature to monitor would not be trivial, as the evoked dynamics are differing between cortical areas and individuals (Figure 3) (Harquel et al., 2016a; Raffin et al., 2020). Assessing input-output curves for every target could be a solution to study the influence of stimulation intensity on the resulting spatial resolution (Raffin et al., 2020). Finally, E-field estimations could also be performed *a priori* to determine the lowest stimulation intensity that efficiently stimulates the cortex, while estimating the spacing between targets to minimize overlapping between E-fields.

5. Conclusions

We explored the spatial resolution of TMS-EEG coupling, which remains unknown to date. By analyzing the evoked dynamics of cortical targets over the sensorimotor cortex, we showed that this technique was able to differentiate responses from site as close as 10 mm. In accordance with the TMS induced E-field modeling, the spatial resolution appeared to be anisotropic and common dynamical signatures were found especially between sites within the same Brodmann area. Such insights about

the spatial resolution of TMS-EEG are important to support future studies based on the spatial specificity of TEPs.

Data and code availability

The data recorded for this study are not publicly available due to absence of public data sharing statement in the informed consent form signed by the participant. The data may be available on request from the corresponding author [BP], on the condition that a data sharing agreement between the academic buyer and Grenoble University Hospital is established. The EEG data analysis function used in this work (using Matlab and Fieldtrip toolbox) can be found here: https://gricad-gitlab.univ-grenoble-alpes.fr/harquels/public_codes.

Declaration of Competing Interest

None.

Credit authorship contribution statement

Brice Passera: Conceptualization, Methodology, Investigation, Formal analysis, Writing – original draft, Visualization. **Alan Chauvin:** Methodology, Formal analysis, Writing – review & editing, Supervision. **Estelle Raffin:** Conceptualization, Writing – review & editing, Visualization. **Thierry Bougerol:** Resources, Project administration. **Olivier David:** Conceptualization, Writing – review & editing, Supervision, Funding acquisition. **Sylvain Harquel:** Conceptualization, Methodology, Investigation, Formal analysis, Writing – original draft, Visualization, Supervision.

Acknowledgments

This work was funded by the Agence Nationale pour la Recherche grant "ANR-15-CE37-0015-1" and by NeuroCoG IDEX UGA in the framework of the "Investissements d'avenir" program (ANR-15-IDEX-02). Data were acquired on a platform of France Life Imaging Network partly funded by the grant "ANR-11-INBS-0006."

Supplementary materials

Supplementary material associated with this article can be found, in the online version, at doi:10.1016/j.neuroimage.2022.119419.

References

Aberra, A.S., Wang, B., Grill, W.M., Peterchev, A.V., 2020. Simulation of transcranial magnetic stimulation in head model with morphologically-realistic cortical neurons. Brain Stimul. 13, 175–189. doi:10.1016/j.brs.2019.10.002.

Arnaldi, D., De Carli, F., Famà, F., Brugnolo, A., Girtler, N., Picco, A., Pardini, M., Accardo, J., Proietti, L., Massa, F., Bauckneht, M., Morbelli, S., Sambuceti, G., Nobili, F., 2022. Prediction of cognitive worsening in de novo Parkinson's disease: clinical use of biomarkers. Mov. Disord. doi:10.1002/mds.27190, n/a-n/a.

Awiszus, F., 2003. Chapter 2 TMS and threshold hunting. Suppl. Clin. Neurophysiol. 56, 13–23. doi:10.1016/S1567-424X(09)70205-3.

Bagattini, C., Mutanen, T.P., Fracassi, C., Manenti, R., Cotelli, M., Ilmoniemi, R.J., Miniussi, C., Bortoletto, M., 2019. Predicting Alzheimer's disease severity by means of TMS–EEG coregistration. Neurobiol. Aging 80, 38–45. doi:10.1016/j.neurobiolaging.2019.04.008.

Baillet, S., Mosher, J.C., Leahy, R.M., 2001. Electromagnetic brain mapping. IEEE Signal Process. Mag. 18, 14–30. doi:10.1109/79.962275.

Bauer, P.R., de Goede, A.A., ter Braack, E.M., van Putten, M.J.A.M., Gill, R.D., Sander, J.W., 2017. Transcranial magnetic stimulation as a biomarker for epilepsy. Brain 140, e18. doi:10.1093/brain/aww345.

Belardinelli, P., Biabani, M., Blumberger, D.M., Bortoletto, M., Casarotto, S., David, O., Desideri, D., Etkin, A., Ferrarelli, F., Fitzgerald, P.B., Fornito, A., Gordon, P.C., Gosseries, O., Harquel, S., Julkunen, P., Keller, C.J., Kimiskidis, V.K., Lioumis, P., Miniussi, C., Rosanova, M., Rossi, S., Sarasso, S., Wu, W., Zrenner, C., Daskalakis, Z.J., Rogasch, N.C., Massimini, M., Ziemann, U., Ilmoniemi, R.J., 2019. Reproducibility in TMS–EEG studies: a call for data sharing, standard procedures and effective experimental control. Brain Stimul. Basic Transl. Clin. Res. Neuromodulation 12, 787–790. doi:10.1016/j.brs.2019.01.010.

Berlim, M.T., McGirr, A., Rodrigues dos Santos, N., Tremblay, S., Martins, R., 2017. Efficacy of theta burst stimulation (TBS) for major depression: An exploratory meta-analysis of randomized and sham-controlled trials. J. Psychiatr. Res. 90, 102–109. doi:10.1016/j.jpsychires.2017.02.015.

Bertazzoli, G., Esposito, R., Mutanen, T.P., Ferrari, C., Ilmoniemi, R.J., Miniussi, C., Bortoletto, M., 2021. The impact of artifact removal approaches on TMS–EEG signal. bioRxiv 2021.01.15.426817. doi:10.1101/2021.01.15.426817.

Biabani, M., Fornito, A., Mutanen, T.P., Morrow, J., Rogasch, N.C., 2019. Characterizing and minimizing the contribution of sensory inputs to TMS-evoked potentials. Brain Stimul. 12, 1537–1552. doi:10.1016/j.brs.2019.07.009.

Bridwell, D.A., Cavanagh, J.F., Collins, A.G.E., Nunez, M.D., Srinivasan, R., Stober, S., Calhoun, V.D., 2018. Moving beyond ERP components: A selective review of approaches to integrate EEG and behavior 12. doi:10.3389/fnhum.2018.00106.

Bungert, A., Antunes, A., Espenhahn, S., Thielscher, A., 2017. Where does TMS stimulate the motor cortex? Combining electrophysiological measurements and realistic field estimates to reveal the affected cortex position. Cereb. Cortex 27, 5083–5094. doi:10.1093/cercor/bhw292.

Burle, B., Spieser, L., Roger, C., Casini, L., Hasbroucq, T., Vidal, F., 2015. Spatial and temporal resolutions of EEG: Is it really black and white? A scalp current density view. Int. J. Psychophysiol. 97, 210–220. doi:10.1016/j.ijpsycho.2015.05.004.

Casarotto, S., Fecchio, M., Rosanova, M., Varone, G., D'Ambrosio, S., Sarasso, S., Pigorini, A., Russo, S., Comanducci, A., Ilmoniemi, R.J., Massimini, M., 2022. The rt-TEP tool: real-time visualization of TMS-Evoked Potentials to maximize cortical activation and minimize artifacts. J. Neurosci. Methods 370, 109486. doi:10.1016/j.jneumeth.2022.109486.

Casarotto, S., Lauro, L.J.R., Bellina, V., Casali, A.G., Rosanova, M., Pigorini, A., Defendi, S., Mariotti, M., Massimini, M., 2010. EEG responses to TMS are sensitive to changes in the perturbation parameters and repeatable over time. PLOS ONE 5, e10281. doi:10.1371/journal.pone.0010281.

Casarotto, S., Turco, F., Comanducci, A., Perretti, A., Marotta, G., Pezzoli, G., Rosanova, M., Isaias, I., 2018. Excitability of the supplementary motor area in Parkinson's disease depends on subcortical damage. Brain Stimulat 12. doi:10.1016/j.brs.2018.10.011.

Caulfield, K., Savoca, M., Lopez, J., Summers, P., Li, X., Fecchio, M., Casarotto, S., Massimini, M., George, M., 2020. Assessing the Intra- and Inter-Subject Reliability of the Perturbational Complexity Index (PCI) of Consciousness for Three Brain Regions Using TMS-EEG doi:10.1101/2020.01.08.898775.

Colella, M., Laher, R.M., Press, D.Z., McIlduff, C.E., Rutkove, S.B., Pascual-Leone, A., Apollonio, F., Liberti, M., Bonmassar, G., 2019. Ultra-focal magnetic stimulation using a μTMS coil: a computational study. In: Annu. Int. Conf. IEEE Eng. Med. Biol. Soc. IEEE Eng. Med. Biol. Soc. Annu. Int. Conf. 2019, pp. 3987–3990. doi:10.1109/EMBC.2019.8857349.

Conde, V., Tomasevic, L., Akopian, I., Stanek, K., Saturnino, G.B., Thielscher, A., Bergmann, T.O., Siebner, H.R., 2018. The non-transcranial TMS-evoked potential is an inherent source of ambiguity in TMS-EEG studies. doi:10.1101/337782.

Darmani, G., Ziemann, U., 2019. Pharmacophysiology of TMS-evoked EEG potentials: a mini-review. Brain Stimulat 12, 829–831. doi:10.1016/j.brs.2019.02.021.

Dubbioso, R., Madsen, K., Thielscher, A., Siebner, H., 2020. Multimodal fingerprinting of the human precentral cortex forming the motor hand knob. doi:10.1101/2020.02.11.942771.

Esser, S.K., Huber, R., Massimini, M., Peterson, M.J., Ferrarelli, F., Tononi, G., 2006. A direct demonstration of cortical LTP in humans: a combined TMS/EEG study. Brain Res. Bull. 69, 86–94. doi:10.1016/j.brainresbull.2005.11.003.

Farzan, F., Vernet, M., Shafi, M.M.D., Rotenberg, A., Daskalakis, Z.J., Pascual-Leone, A., 2016. Characterizing and Modulating Brain Circuitry through Transcranial Magnetic Stimulation Combined with Electroencephalography. Front. Neural Circuits 10. doi:10.3389/fncir.2016.00073.

Fecchio, M., Pigorini, A., Comanducci, A., Sarasso, S., Casarotto, S., Premoli, I., Derchi, C.-C., Mazza, A., Russo, S., Resta, F., Ferrarelli, F., Mariotti, M., Ziemann, U., Massimini, M., Rosanova, M., 2017. The spectral features of EEG responses to transcranial magnetic stimulation of the primary motor cortex depend on the amplitude of the motor evoked potentials. PLoS ONE 12. doi:10.1371/journal.pone.0184910.

Freedberg, M., Reeves, J.A., Hussain, S.J., Zaghloul, K.A., Wassermann, E.M., 2020. Identifying site- and stimulation-specific TMS-evoked EEG potentials using a quantitative cosine similarity metric. PloS One 15, e0216185. doi:10.1371/journal.pone.0216185.

Harquel, S., Bacle, T., Beynel, L., Marendaz, C., Chauvin, A., David, O., 2016a. Mapping dynamical properties of cortical microcircuits using robotized TMS and EEG: Towards functional cytoarchitectonics. NeuroImage 135, 115–124. doi:10.1016/j.neuroimage.2016.05.009.

Harquel, S., Beynel, L., Guyader, N., Marendaz, C., David, O., Chauvin, A., 2016b. CortEx-Tool: a toolbox for processing motor cortical excitability measurements by transcranial magnetic stimulation.

Harquel, S., Diard, J., Raffin, E., Passera, B., Dall'Igna, G., Marendaz, C., David, O., Chauvin, A., 2017. Automatized set-up procedure for transcranial magnetic stimulation protocols. NeuroImage 153, 307–318. doi:10.1016/j.neuroimage.2017.04.001.

Heuvel, M.P.van den, Scholtens, L.H., Barrett, L.F., Hilgetag, C.C., Reus, M.A.de, 2015. Bridging cytoarchitectonics and connectomics in human cerebral cortex. J. Neurosci. 35, 13943–13948. doi:10.1523/JNEUROSCI.2630-15.2015.

Janssen, A.M., Oostendorp, T.F., Stegeman, D.F., 2014. The effect of local anatomy on the electric field induced by TMS: evaluation at 14 different target sites. Med. Biol. Eng. Comput. 52, 873–883. doi:10.1007/s11517-014-1190-6.

Komssi, S., Kähkönen, S., Ilmoniemi, R.J., 2004. The effect of stimulus intensity on brain responses evoked by transcranial magnetic stimulation. Hum. Brain Mapp. 21, 154–164. doi:10.1002/hbm.10159.

Konakanchi, D., de Jongh Curry, A.L., Waters, R.S., Narayana, S., 2020. Focality of the induced E-field is a contributing factor in the choice of TMS Parameters: Evidence from a

3D computational model of the human brain. Brain Sci 10, E1010. doi:10.3390/brainsci10121010.
Lioumis, P., Kičić, D., Savolainen, P., Mäkelä, J.P., Kähkönen, S., 2009. Reproducibility of TMS—evoked EEG responses. Hum. Brain Mapp. 30, 1387–1396. doi:10.1002/hbm.20608.
Makarov, S.N., Wartman, W.A., Noetscher, G.M., Fujimoto, K., Zaidi, T., Burnham, E.H., Daneshzand, M., Nummenmaa, A., 2021. Degree of improving TMS focality through a geometrically stable solution of an inverse TMS problem. NeuroImage 241, 118437. doi:10.1016/j.neuroimage.2021.118437.
Meincke, J., Hewitt, M., Batsikadze, G., Liebetanz, D., 2016. Automated TMS hotspot-hunting using a closed loop threshold-based algorithm. NeuroImage 124 (Part A), 509–517. doi:10.1016/j.neuroimage.2015.09.013.
Morris, T., Engelbertson, A., Guidice, W., 2020. Repetitive transcranial magnetic stimulation (rTMS): a large-scale retrospective clinical data analysis indicating rTMS as effective treatment for generalized anxiety disorder (GAD). Brain Stimul. Basic Transl. Clin. Res. Neuromodul. 13, 1843. doi:10.1016/j.brs.2020.06.021.
Mutanen, T., Mäki, H., Ilmoniemi, R.J., 2013. The effect of stimulus parameters on TMS–EEG muscle artifacts. Brain Stimulat 6, 371–376. doi:10.1016/j.brs.2012.07.005.
Nielsen, J.D., Madsen, K.H., Puonti, O., Siebner, H.R., Bauer, C., Madsen, C.G., Saturnino, G.B., Thielscher, A., 2018. Automatic skull segmentation from MR images for realistic volume conductor models of the head: assessment of the state-of-the-art. NeuroImage 174, 587–598. doi:10.1016/j.neuroimage.2018.03.001.
Oostenveld, R., Fries, P., Maris, E., Schoffelen, J.-M., 2011. FieldTrip: open source software for advanced analysis of MEG, EEG, and invasive electrophysiological data. Comput. Intell. Neurosci. 2011, e156869. doi:10.1155/2011/156869.
Opitz, A., Windhoff, M., Heidemann, R.M., Turner, R., Thielscher, A., 2011. How the brain tissue shapes the electric field induced by transcranial magnetic stimulation. NeuroImage 58, 849–859. doi:10.1016/j.neuroimage.2011.06.069.
Pascual-Leone, A., Freitas, C., Oberman, L., Horvath, J.C., Halko, M., Eldaief, M., Bashir, S., Vernet, M., Shafi, M., Westover, B., Vahabzadeh-Hagh, A.M., Rotenberg, A., 2011. Characterizing brain cortical plasticity and network dynamics across the age-span in health and disease with TMS-EEG and TMS-fMRI. Brain Topogr 24, 302–315. doi:10.1007/s10548-011-0196-8.
Premoli, I., Bergmann, T.O., Fecchio, M., Rosanova, M., Biondi, A., Belardinelli, P., Ziemann, U., 2017. The impact of GABAergic drugs on TMS-induced brain oscillations in human motor cortex. NeuroImage 163, 1–12. doi:10.1016/j.neuroimage.2017.09.023.
Premoli, I., Castellanos, N., Rivolta, D., Belardinelli, P., Bajo, R., Zipser, C., Espenhahn, S., Heidegger, T., Müller-Dahlhaus, F., Ziemann, U., 2014. TMS-EEG signatures of GABAergic neurotransmission in the human cortex. J. Neurosci. 34, 5603–5612. doi:10.1523/JNEUROSCI.5089-13.2014.
Raffin, E., Harquel, S., Passera, B., Chauvin, A., Bougerol, T., David, O., 2020. Probing regional cortical excitability via input–output properties using transcranial magnetic stimulation and electroencephalography coupling. Hum. Brain Mapp. 41, 2741–2761. doi:10.1002/hbm.24975.
Raffin, E., Pellegrino, G., Di Lazzaro, V., Thielscher, A., Siebner, H.R., 2015. Bringing transcranial mapping into shape: Sulcus-aligned mapping captures motor somatotopy in human primary motor hand area. NeuroImage 120, 164–175. doi:10.1016/j.neuroimage.2015.07.024.
Rehn, S., Eslick, G.D., Brakoulias, V., 2018. A meta-analysis of the effectiveness of different cortical targets used in repetitive transcranial magnetic stimulation (rTMS) for the treatment of obsessive-compulsive disorder (OCD). Psychiatr. Q. 89, 645–665. doi:10.1007/s11126-018-9566-7.
Reijonen, J., Pitkänen, M., Kallioniemi, E., Mohammadi, A., Ilmoniemi, R., Julkunen, P., 2020. Spatial extent of cortical motor hotspot in navigated transcranial magnetic stimulation. J. Neurosci. Methods 346, 108893. doi:10.1016/j.jneumeth.2020.108893.
Rogasch, N.C., Sullivan, C., Thomson, R.H., Rose, N.S., Bailey, N.W., Fitzgerald, P.B., Farzan, F., Hernandez-Pavon, J.C., 2017. Analysing concurrent transcranial magnetic stimulation and electroencephalographic data: A review and introduction to the open-source TESA software. NeuroImage 147, 934–951. doi:10.1016/j.neuroimage.2016.10.031.
Rogasch, N.C., Thomson, R.H., Farzan, F., Fitzgibbon, B.M., Bailey, N.W., Hernandez-Pavon, J.C., Daskalakis, Z.J., Fitzgerald, P.B., 2014. Removing artefacts from TMS-EEG recordings using independent component analysis: Importance for assessing prefrontal and motor cortex network properties. NeuroImage 101, 425–439. doi:10.1016/j.neuroimage.2014.07.037.
Romero, M.C., Davare, M., Armendariz, M., Janssen, P., 2019. Neural effects of transcranial magnetic stimulation at the single-cell level. Nat. Commun. 10, 2642. doi:10.1038/s41467-019-10638-7.
Roos, D., Biermann, L., Jarczok, T.A., Bender, S., 2021. Local differences in cortical excitability – a systematic mapping study of the TMS-evoked N100 component. Front. Neurosci. 15. doi:10.3389/fnins.2021.623692.
Rosanova, M., Casali, A., Bellina, V., Resta, F., Mariotti, M., Massimini, M., 2009. Natural frequencies of human corticothalamic circuits. J. Neurosci. 29, 7679–7685. doi:10.1523/JNEUROSCI.0445-09.2009.
Rossi, S., Pasqualetti, P., Tecchio, F., Sabato, A., Rossini, P.M., 1998. Modulation of corticospinal output to human hand muscles following deprivation of sensory feedback. NeuroImage 8, 163–175. doi:10.1006/nimg.1998.0352.
Rossini, P.M., Barker, A.T., Berardelli, A., Caramia, M.D., Caruso, G., Cracco, R.Q., Dimitrijević, M.R., Hallett, M., Katayama, Y., Lücking, C.H., Maertens de Noordhout, A.L., Marsden, C.D., Murray, N.M.F., Rothwell, J.C., Swash, M., Tomberg, C., 1994. Non-invasive electrical and magnetic stimulation of the brain, spinal cord and roots: basic principles and procedures for routine clinical application. Report of an IFCN committee. Electroencephalogr. Clin. Neurophysiol. 91, 79–92. doi:10.1016/0013-4694(94)90029-9.
Rossini, P.M., Burke, D., Chen, R., Cohen, L.G., Daskalakis, Z., Di Iorio, R., Di Lazzaro, V., Ferreri, F., Fitzgerald, P.B., George, M.S., Hallett, M., Lefaucheur, J.P., Langguth, B., Matsumoto, H., Miniussi, C., Nitsche, M.A., Pascual-Leone, A., Paulus, W., Rossi, S., Rothwell, J.C., Siebner, H.R., Ugawa, Y., Walsh, V., Ziemann, U., 2015. Non-invasive electrical and magnetic stimulation of the brain, spinal cord, roots and peripheral nerves: Basic principles and procedures for routine clinical and research application. An updated report from an I.F.C.N. Committee. Clin. Neurophysiol. Off. J. Int. Fed. Clin. Neurophysiol. 126, 1071–1107. doi:10.1016/j.clinph.2015.02.001.
Rousset, F., Ferdy, J.-B., 2014. Testing environmental and genetic effects in the presence of spatial autocorrelation. Ecography 37, 781–790. doi:10.1111/ecog.00566.
RStudio Team, 2019. RStudio: Integrated Development for R. RStudio, Inc., Boston, MA URL.
Säisänen, L., Könönen, M., Niskanen, E., Lakka, T., Lintu, N., Vanninen, R., Julkunen, P., Määttä, S., 2021. Primary hand motor representation areas in healthy children, preadolescents, adolescents, and adults. NeuroImage 228, 117702. doi:10.1016/j.neuroimage.2020.117702.
Saturnino, G.B., Puonti, O., Nielsen, J.D., Antonenko, D., Madsen, K.H., Thielscher, A., 2019. SimNIBS 2.1: a comprehensive pipeline for individualized electric field modelling for transcranial brain stimulation. In: Makarov, S., Horner, M., Noetscher, G. (Eds.), Brain and Human Body Modeling: Computational Human Modeling at EMBC 2018. Springer International Publishing, Cham, pp. 3–25. doi:10.1007/978-3-030-21293-3_1.
Siebner, H.R., Conde, V., Tomasevic, L., Thielscher, A., Bergmann, T.O., 2019. Distilling the essence of TMS-evoked EEG potentials (TEPs): A call for securing mechanistic specificity and experimental rigor. Brain Stimul. Basic Transl. Clin. Res. Neuromodulation 12, 1051–1054. doi:10.1016/j.brs.2019.03.076.
Stokes, M.G., Chambers, C.D., Gould, I.C., English, T., McNaught, E., McDonald, O., Mattingley, J.B., 2007. Distance-adjusted motor threshold for transcranial magnetic stimulation. Clin. Neurophysiol. 118, 1617–1625. doi:10.1016/j.clinph.2007.04.004.
Tadel, F., Baillet, S., Mosher, J.C., Pantazis, D., Leahy, R.M., 2011. Brainstorm: a user-friendly application for MEG/EEG analysis [WWW Document]. Comput. Intell. Neurosci. doi:10.1155/2011/879716.
ter Braack, E.M., de Vos, C.C., van Putten, M.J.A.M., 2015. Masking the auditory evoked potential in TMS–EEG: a comparison of various methods. Brain Topogr 28, 520–528. doi:10.1007/s10548-013-0312-z.
The jamovi project, 2020. jamovi (Version 1.2) [Computer Software] Retrieved from.
Thielscher, A., Antunes, A., Saturnino, G.B., 2015. Field modeling for transcranial magnetic stimulation: A useful tool to understand the physiological effects of TMS? In: Annual International Conference of the IEEE Engineering in Medicine and Biology Society IEEE Eng. Med. Biol. Soc. Annu. Int. Conf. 2015, pp. 222–225. doi:10.1109/EMBC.2015.7318340.
Tremblay, S., Rogasch, N., Premoli, I., Blumberger, D., Casarotto, S., Chen, R., Di Lazzaro, V., Farzan, F., Ferrarelli, F., Fitzgerald, P., Hui, J., Ilmoniemi, R., Kimiskidis, V., Kugiumtzis, D., Lioumis, P., Pascual-Leone, A., Pellicciari, M.C., Rajji, T., Thut, G., Daskalakis, Z., 2019. Clinical utility and prospective of TMS–EEG. Clin. Neurophysiol. 130. doi:10.1016/j.clinph.2019.01.001.
Valero-Cabré, A., Amengual, J.L., Stengel, C., Pascual-Leone, A., Coubard, O.A., 2017. Transcranial magnetic stimulation in basic and clinical neuroscience: a comprehensive review of fundamental principles and novel insights. Neurosci. Biobehav. Rev. 83, 381–404. doi:10.1016/j.neubiorev.2017.10.006.
van de Ruit, M., Perenboom, M.J.L., Grey, M.J., 2015. TMS brain mapping in less than two minutes. Brain Stimul. 8, 231–239. doi:10.1016/j.brs.2014.10.020.
Veniero, D., Bortoletto, M., Miniussi, C., 2013. Cortical modulation of short-latency TMS-evoked potentials. Front. Hum. Neurosci. 6. doi:10.3389/fnhum.2012.00352.
Wassermann, E., Epstein, C., Ziemann, U., Walsh, V., Paus, T., Lisanby, S. (Eds.), 2008. Oxford Handbook of Transcranial Stimulation, Oxford Library of Psychology. Oxford University Press, Oxford, New York.
Woźniak-Kwaśniewska, A., Szekely, D., Aussedat, P., Bougerol, T., David, O., 2014. Changes of oscillatory brain activity induced by repetitive transcranial magnetic stimulation of the left dorsolateral prefrontal cortex in healthy subjects. NeuroImage 88, 91–99. doi:10.1016/j.neuroimage.2013.11.029.
Ziemann, U., Reis, J., Schwenkreis, P., Rosanova, M., Strafella, A., Badawy, R., Müller-Dahlhaus, F., 2015. TMS and drugs revisited 2014. Clin. Neurophysiol. 126, 1847–1868. doi:10.1016/j.clinph.2014.08.028.